Theoretical Description of the Structure and Magnetic Properties of Nitroxide−Cu(II)−Nitroxide Spin Triads by Means of Multiconfigurational Ab Initio Calculations

Steven Vancoillie,[†] Lubomír Rulíšek,[‡] Frank Neese,[§] and Kristine Pierloot*[,†]

Department of Chemistry, University of Leuven, Celestijnenlaan 200F, B-3001 Heverlee-Leuven, Belgium, Institute of Organic Chemistry and Biochemistry, Academy of Sciences of the Czech Republic, and Gilead Sciences Research Center at IOCB, Flemingovo nam. 2, 166 10 Praha 6, Czech Republic, and Institut für Pysikalische and Theoretische Chemie, Universität Bonn, Wegelerstrasse 12, D-53115 Bonn, Germany

Received: January 28, 2009; Revised Manuscript Received: March 17, 2009

The structural, electronic and magnetic properties of two different models of the heterospin polymer chain complexes of Cu^{2+} hexafluoroacetylacetonate with two pyrazole-substituted nitronyl nitroxides $Cu(hfac)_2L^R$ have been studied by means of multiconfigurational perturbation theory based on a CASSCF (complete active space self-consistent field) wave function, i.e. the CASPT2 method. Our calculations reveal the presence of two minima in the electronic energy curve along the $Cu-O_L$ bond, separated by only 6 kcal/mol, and corresponding to the X-ray structures of the CuO_6 centers in $Cu(hfac)_2L^{Pr}$ at 115 and 293 K, respectively. The two energetic minima are characterized by a different electronic structure, thus giving rise to a different three-spin exchange coupling and explaining the thermally induced spin transitions in this family of compounds. The concomitant variations in the magnetic properties, i.e. g factors and magnetic moments $\mu_{eff}(T)$ were calculated and compared with the experimental data of $Cu(hfac)_2L^{Pr}$. Even if the correspondence is only qualitative, our calculations provide a convincing explanation of the observed magnetic peculiarities. In particular, at low temperatures, the predicted ground-state is ^2A_u, well separated from the ^2A_g, ^4A_u states and therefore exclusively populated. Its calculated g factors, $g_{||} = 1.848$, $g_{\perp} = 1.965$, 1.974, qualitatively correspond to the observed $g < 2$ signals in the low-temperature EPR spectra. The previously assumed formal spin assignment >N−O$^{\bullet}$−Cu−$^{\bullet}$O−N< for these linear spin triads is challenged by our calculations, pointing instead to a more important role of the end-standing NO in the exchange interactions with Cu(II).

1. Introduction

During the last decades, exchange-coupled complexes between transition metal ions and stable organic radicals have gained significant popularity in the field of molecular magnetism. In this respect, a new family of heterospin polymer-chain complexes of Cu^{2+} hexafluoroacetylacetonato $Cu(hfac)_2$ with stable pyrazole-substituted nitronyl nitroxides (L^R) has recently been proposed.[1–6] These so-called "breathing crystals" have been found to exhibit structural rearrangements at low temperatures giving rise to magnetic anomalies in the temperature dependence of the effective magnetic moment, similar to classical spin-crossover. The character of the magnetic anomalies is strongly dependent on the substituent R of the nitroxide ligand[1,3] and on the character of the solvent molecules in the interchain space.[6] The thermally induced structural changes and conjugated spin transitions were studied previously using X-ray diffraction, EPR, and magnetic susceptibility techniques.[1–6] Moreover, in a recent study on breathing crystals $Cu(hfac)_2L^{Pr}$ (Pr = propyl) it was shown that the same type of spin transition may also be induced by light irradiation.[7]

The present contribution aims at providing a theoretical description of the observed structural and magnetic phenomena, based on multiconfigurational ab initio calculations on complexes modeling one nitroxide−copper(II)−nitroxide spin triad occurring in $Cu(hfac)_2L^R$ crystals with a head-to-head polymer chain motif.[1] Such polymer chains contain alternating three-spin CuO_6 and one-spin CuO_4N_2 units. The CuO_6 complex considered in the present study is $Cu(hfac)_2L^{Pr}$, for which X-ray structural data are available[1] and experimental magnetic and EPR studies were reported.[1–5] This complex will be denoted as model II in the rest of this work, and is shown in Figure 1B. Most of our calculations were, however, performed on a simplified CuO_6 complex, denoted as model I and shown in Figure 1A, consisting of Cu^{2+} hexafluoroacetylacetonate $Cu(hfac)_2$ with two axial nitronyl nitroxides, but with the pyrazole substituents of the nitroxides omitted and replaced by hydrogen. For both models, g factors and magnetic moments at different temperatures are obtained by making use of the CASPT2 method[8] (multiconfigurational perturbation theory based on a complete active space SCF wave function) including spin−orbit coupling.[9] These calculations are performed on structures obtained from geometry optimizations by means of DFT (density functional theory).

The theoretical description provided in this work will necessarily be qualitative, ignoring any effect related to the presence of varying R substituents. Moreover, since only the CuO_6 unit is included in our models, contributions of the one-spin CuO_4N_2 unit to the observed EPR spectra and experimentally measured magnetic moment are not calculated. Intercluster exchange coupling between the three-spin and one-spin units

* Corresponding author. Fax: +32 16 32 79 92. E-mail: Kristin.Pierloot@chem.kuleuven.be.
[†] University of Leuven.
[‡] Academy of Sciences of the Czech Republic and Gilead Sciences Research Center at IOCB.
[§] Universität Bonn.

10.1021/jp900822v CCC: $40.75
Published on Web 05/04/2009

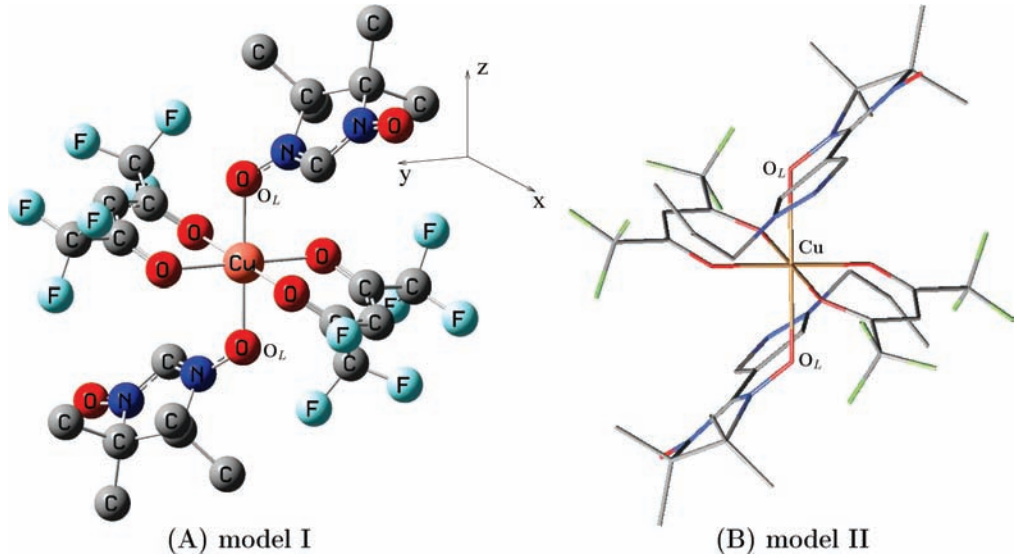

Figure 1. Calculated cluster models. Hydrogens are omitted for clarity.

in the polymer chain is also ignored, but it was found to be smaller by at least 1 order of magnitude than the intracluster exchange interaction.[5]

2. Computational Details

2.1. DFT Calculations. For the simplest model I, shown in Figure 1A, a series of DFT geometry optimizations was first performed. C_i symmetry was maintained during the structure optimizations, and all calculations were performed for the lowest high-spin ^4A_u state. All but one geometrical parameter were optimized. The fixed parameter concerns the distance Cu−O_L between the copper and the nitroxide oxygens O_L. This distance was varied between 1.90 and 2.33 Å, with steps of 0.02 Å or less (around the critical points).

For the Cu(hfac)$_2$L^{Pr} complex (model II, see Figure 1B) two DFT structures were calculated, starting from the experimental crystal data[1] at 115 and 293 K and keeping the Cu−O distances fixed [at R(Cu−O_L) = 2.018 Å, R(Cu−O_x) = 2.263 Å, R(Cu−O_y) = 1.959 Å for the 115 K structure and at R(Cu−O_L) = 2.318 Å, R(Cu−O_x) = 1.955 Å, R(Cu−O_y) = 1.975 Å for the 293 K structure], while optimizing all other structural parameters. Also in this case, the optimization was performed for the ^4A_u state.

All DFT calculations were performed with the Turbomole code,[10] making use of the PBE0 functional[11,12] and with basis sets denoted as def2-SVP in Turbomole.[13]

2.2. CASPT2 Calculations. Single-point CASSCF/CASPT2 calculations[8] were subsequently performed on each of the structures obtained from DFT. ANO-s type basis sets[14] were used in these calculations, contracted as [6s4p3d2f] for copper, [3s2p1d] for all nitrogens and oxygens as well as for the carbon atoms belonging to the axial nitroxide rings. The d polarization function was omitted for all other carbon atoms and also for the fluorines of the hfac ligands, thus giving [3s2p] for these atoms. All hydrogens were described by means of a [2s] contracted set. An imaginary level shift[15] of 0.1 au was used in all CASPT2 calculations to improve convergence and avoid intruder states. All CASPT2 calculations were performed with the Molcas software.[16]

A first series of two-state CASPT2 calculations was performed on model I, making use of the stuctures obtained from DFT. These calculations were based on an average CASSCF calculation on the lowest two states of each of the representations ^2A_u, ^2A_g, and ^4A_u. CASSCF reference wave functions were obtained by distributing 11 electrons in 12 active orbitals: five Cu 3d orbitals and a correlating Cu 3d′ shell and the a_g and a_u combinations of the nitroxide NOπ* orbitals. For the CASPT2 calculations on the different DFT structures of model I, the original zeroth-order Hamiltonian[8] was used. All core electrons (up to Cu 3s,3p) were frozen during the CASPT2 calculations. From these CASPT2 calculations, two local structural minima were obtained, corresponding to a Cu−O_{XL} distance of 1.946 and 2.191 Å.

In order to obtain g factors and magnetic moments, a second set of CASPT2 calculations was performed, now including all ligand field states (five for each spin and symmetry). For these calculations, the active space was extended with one doubly occupied orbital, so as to give a (13 in 13) active space. The orbital concerned is the bonding counterpart of the singly occupied Cu 3d orbital (either $d_{y^2-z^2}$ or $d_{x^2-y^2}$; see further) in the lowest ^2A_u, ^2A_g, and ^4A_u states of each structure. Inclusion of the bonding orbital into the active space serves to provide an improved description of the covalency of the Cu−O bonds at the CASSCF level,[17−19] which is of particular importance for the calculation of the **g** tensors,[20] described in the next section.

CASPT2 calculations based on a (13 in 13) active space were performed on the two minimal energy structures for model I and on the structures obtained from DFT for model II. For the smaller model I, all valence electrons were included in the CASPT2 correlation treatment. On the other hand, for the large model II, including the entire valence orbital space would lead to very time-consuming calculations, and it was also felt to be unnecessary, as correlation of electrons confined to regions distant from the magnetic center (e.g., the Pr substituents) may be expected not to influence the calculated magnetic properties to a significant extent. Therefore, a localization procedure was applied to the inactive orbitals, after which the correlation orbital space was limited to orbitals with a density contribution of at least 0.1/au^2 in the central region, consisting of copper, the two equatorial OCCCO bidentates (not including the CF_3 substituents), and the axial nitronyl nitroxides (not including their substituents).

In the CASPT2 treatment, two different types of zeroth-order Hamiltonians were considered: the original $\hat{H}^{(0)}$, on the one hand, and the IPEA-modified $\hat{H}^{(0)}$, on the other. The original implementation of CASPT2 in Molcas used a Fock-type $\hat{H}^{(0)}$ that in

the limit of zero active orbitals coincides with the Møller−Plesset zeroth-order Hamiltonian.[8,21] Aiming to repair the systematic underestimation of the energy of *N*-electron states dominated by closed-shell configurations with respect to states dominated by open-shell configurations, the IPEA-modified $\hat{H}^{(0)}$ was introduced[22] and became the standard zeroth-order Hamiltonian in Molcas 6.4. However, in a recent systematic investigation of the applicability of multireference second-order perturbation theory to study magnetic coupling in molecular complexes,[23] it was shown that the IPEA $\hat{H}^{(0)}$ predicts unphysical deviations from the expected regular spacings between the lowest electronic states in the case of weak couplings. This was taken as a good reason to test the quality of both types of $\hat{H}^{(0)}$ in the present case, too.

2.3. Calculation of g Tensors and Magnetic Moments. Calculation of the *g* factors and magnetic moments was performed by making use of the CASSCF state interaction method,[24] as implemented in the Molcas RASSI code, for the calculation of matrix elements between different states, combined with CASPT2 energies. Spin−orbit coupling (SOC) was treated within the manifold of the 15 ligand field states, by means of the RASSI-SOC method[9] making use of AMFI integrals.[25−27] *g* factors were obtained with two different approaches for either the ^2A_u, ^2A_g, or the ^4A_u state. More details of both approaches may be found in ref 28. For the doublet states, the *g* factors were obtained by adding the Zeeman effect through first-order degenerate perturbation theory within the Kramer's doublet obtained after including SOC (approach II in ref 28). For the quartet state, this approach is precluded by the too small (2 cm^{-1} or less) energy splitting between the two doublets resulting from the SOC treatment. Therefore, the *g* factors of this state were instead obtained from a simultaneous treatment of the Zeeman effect and SOC through second-order perturbation theory (approach I in ref 28).

The effective magnetic moment μ_{eff} was calculated from the formula:

$$\mu_{\text{eff}} = \sqrt{\frac{3k}{N_A \beta^2 \mu_0}\chi T}$$

where *k* is Boltzmann's constant, N_A is Avogadro's number, μ_0 is the magnetic constant (vacuum permeability), and β is the Bohr magneton.

The magnetic susceptibility χ is obtained by averaging the eigenvalues of the magnetic susceptibility tensor χ^m_{pq}, which is obtained discretely by calculating the molar magnetization $\mathbf{M}^m$ for different magnitudes and directions of the magnetic field **B** in the linear regime:

$$\chi^m_{pq} = \frac{\Delta M^m_p}{\Delta H_q} = \mu_0 \frac{\Delta M^m_p}{\Delta B_q}$$

The molar magnetization components M^m_p are calculated by applying a Boltzman distribution on the individual magnetic moments, which are the expectation values of the magnetic moment operator within the Zeeman eigenfunctions:

$$M^m_p = -N_A \beta \frac{\sum_i \langle \Psi^{Ze}_i | (L_p + g_e S_p) | \Psi^{Ze}_i \rangle \exp\left(-\frac{E^{Ze}_i}{kT}\right)}{\sum_i \exp\left(-\frac{E^{Ze}_i}{kT}\right)}$$

The Zeeman eigenfunctions are obtained by diagonalizing the Zeeman Hamiltonian within the basis of SO states.

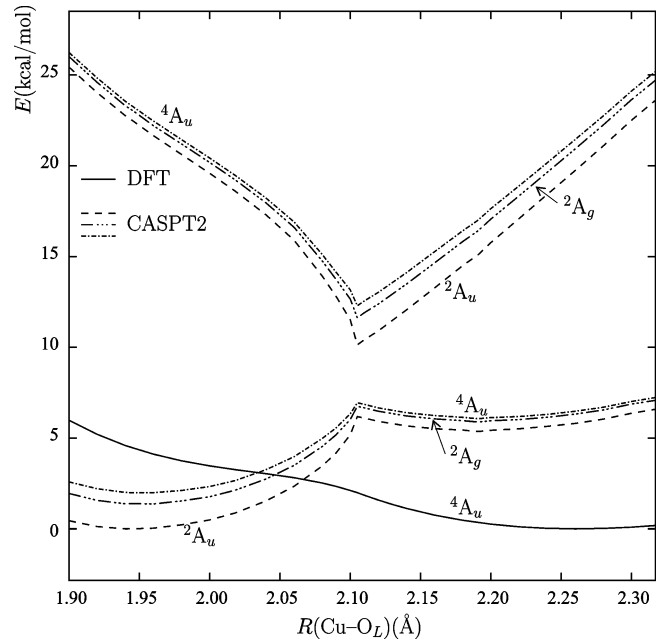

Figure 2. Electronic energy profile along the Cu−O_L axis.

3. Results and Discussion

3.1. Geometrical and Electronic Structure at Low and High Temperature. The Cu(II) ion and the nitroxide ligands each have one unpaired electron. In C_i symmetry, this gives rise to two doublet states (^2A_g and ^2A_u) and one quartet state (^4A_u), for each of the five possible d^9 configurations on copper, thus giving a total of 15 ligand field states. Figure 2 shows the energy curve as a function of the Cu−O_L distance, as obtained from DFT for the lowest ^4A_u state and from CASPT2 for the lowest six of these 15 states. The DFT energy curve shows only one minimum, corresponding to a Cu−O_L distance of 2.26 Å, although an additional plateau is manifested by the energy curve in the 1.95−2.00 Å region. On the other hand, with CASPT2, two minima are observed, occurring at the same Cu−O_L distance for each set of $^2A_{g,u}$, ^4A_u states. The structure with lowest energy is found at a Cu−O_L distance of 1.946 Å. This structure is characterized by one short, 2.003 Å, and one considerably longer Cu−O_{hfac} distance, 2.289 Å. The second minimum occurs at R(Cu−O_L) = 2.191 Å. This structure now has four short Cu−O_{hfac} distances of 1.996−1.997 Å. The CASPT2 energy curves also clearly point to the occurrence of a forbidden crossing between pairs of states with the same spin and symmetry, thus indicating a change of the ground-state electronic structure with an increasing Cu−O_L distance. The crossing occurs at R(Cu−O_L) = 2.11 Å. At longer Cu−O_L distances, the calculated structures correspond to a distorted octahedron with an elongated O_L−Cu−O_L bond, whereas compression of the Cu−O_L bond leads to a gradual increase of one of the Cu−O_{hfac} bonds, thus leading instead to a Jahn−Teller distorted octahedron with one long O_{hfac}−Cu−O_{hfac} axis.

The calculated electronic energy difference between the ground states of both structures amounts to 2100 cm^{-1} or 6 kcal/mol. This indicates that, given favorable entropy factors, the higher-energy structure (long O_L−Cu−O_L axis) might become thermally accessible from the lower-energy structure (long O_{hfac}−Cu−O_{hfac} axis), thus giving rise to temperature-dependent properties, related to a different electronic structure at the two different geometrical structures. In what follows, we will refer to the two structures of model I as respectively low-*T* and high-*T* structure. When comparing the calculated structures

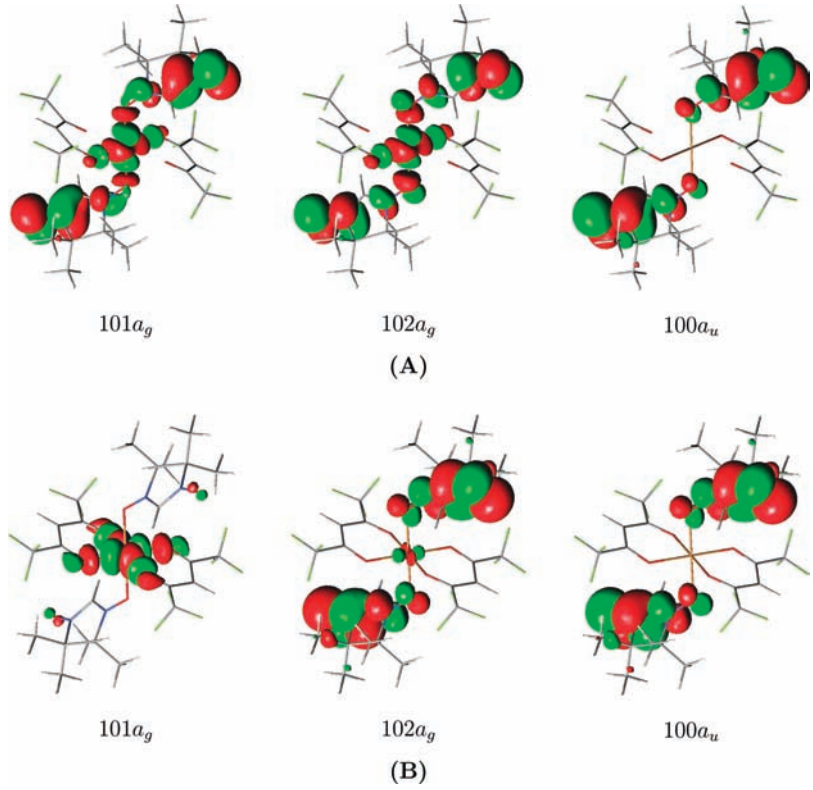

Figure 3. Natural orbitals containing the three unpaired electrons in the lowest ^2A_u, ^2A_g, ^4A_u states of model I: (A) low-*T* structure and (B) high-*T* structure.

of model I to the experimental X-ray structural data of the CuO_6 units in $Cu(hfac)_2L^{Pr}$,[1] an obvious correspondence is found between the low-*T* and high-*T* structure and the crystal structures at respectively 115 and 293 K. At room temperature, these crystals indeed also contain Jahn−Teller distorted octahedral units CuO_6 with a long Cu−O_L distance (2.32 Å) and two short Cu−O_{hfac} distances (1.95, 1.98 Å), whereas on cooling the long O_L−Cu−O_L axis is replaced by one of the O_{hfac}−Cu−O_{hfac} axes, giving at 115 K R(Cu−O_L) = 2.02 Å and R(Cu−O_{hfac}) = 1.96, 2.26 Å. Starting from these crystal structures and keeping all six Cu−O distances fixed at the crystal values, DFT structures for model II were obtained (cf. section 2.1), which will further be denoted as the model II low-*T* and high-*T* structures.

Before considering the magnetic properties of the low-*T* and high-*T* structures of both models, it is instructive to first take a closer look at the electronic stucture of their lowest doublet and quartet states, as illustrated by the composition of the three natural orbitals involved in the exchange interactions (Figure 3) and by their spin densities (Figure 4). The orbitals are taken from the ^2A_u state, using the CAS (13 in 13) results of model I, but essentially the same orbitals are obtained for all three states at the same structure and also for the corresponding model II structures.

As is clearly demonstrated by these plots, the crucial difference in electronic structure between both geometries lies in the character of the Cu(II) singly occupied 3d orbital. With two short Cu−O_L bonds along the *z*-axes and two short Cu−O_{hfac} bonds along the *y*-axes, the Cu 3d orbital involved in the strongest antibonding interaction with the ligands is the $d_{y^2-z^2}$ orbital, which therefore remains singly occupied in the ground state. On the other hand, increasing the Cu−O_L bonds leads to a tetragonal structure in which the Cu $d_{x^2-y^2}$ is singly occupied, since this orbital now forms four σ-bonds with the O_{hfac} ligands in the *xy*-plane. As can also be seen from the orbital plots, a small but distinct overlap of the Cu $d_{y^2-z^2}$ orbital and the gerade NOπ^* combination in the low-*T* structure gives rise to the formation of a positive and negative combination between Cu $3d_{y^2-z^2}$ and the gerade NOπ^* orbital within the representation a_g. On the other hand, in the high-*T* structure, such overlap is absent, and the a_g orbitals essentially remain localized on either copper or NO.

The electronic structure of the ^4A_u state is straightforward, with only one important term in the CASSCF wave function, corresponding to three electrons with equal spin in each of the three natural orbitals. In the ^2A_u state, the a_u NOπ^* orbital is strictly singly occupied. On the other hand, within a_g, one orbital ($101a_g$ in Figure 3) obtains an occupation number slightly higher than 1.0, at the expense of the other orbital ($102a_g$). This points to a weak antiferromagnetic coupling between two single electrons localized on either Cu 3d or on the a_g NOπ^* orbital. The amount of electrons shifted between the two a_g orbitals is significantly larger (0.09 e) in the low-*T* than in the high-*T* structure (0.003 e), suggesting a weaker exchange interaction for the latter structure. The antiferromagnetic coupling scheme is further illustrated by the spin density plots of the ^2A_u state in Figure 4, showing spin-down density on copper antiferromagnetically coupled to spin-up density on both NO. Noteworthy is also that the unpaired electrons of the nitronyl nitroxides are primarily localized in the π^* orbitals of the end-standing NO, not on the ones coordinated to copper. The latter is misleadingly suggested by omitting the end-standing NO is the notation >N−O$^\bullet$−Cu−$^\bullet$O−*N*< used in previous papers on the subject. The NO coordinated to copper are of course still important for the antiferromagnetic interaction, because they are the ones that, by interacting with the copper, deliver the exchange to it. For the ^2A_g state, the spin density plots in Figure 4 point to a different type of exchange coupling, with one unpaired electron residing exclusively in Cu 3d (with a small contribution on its

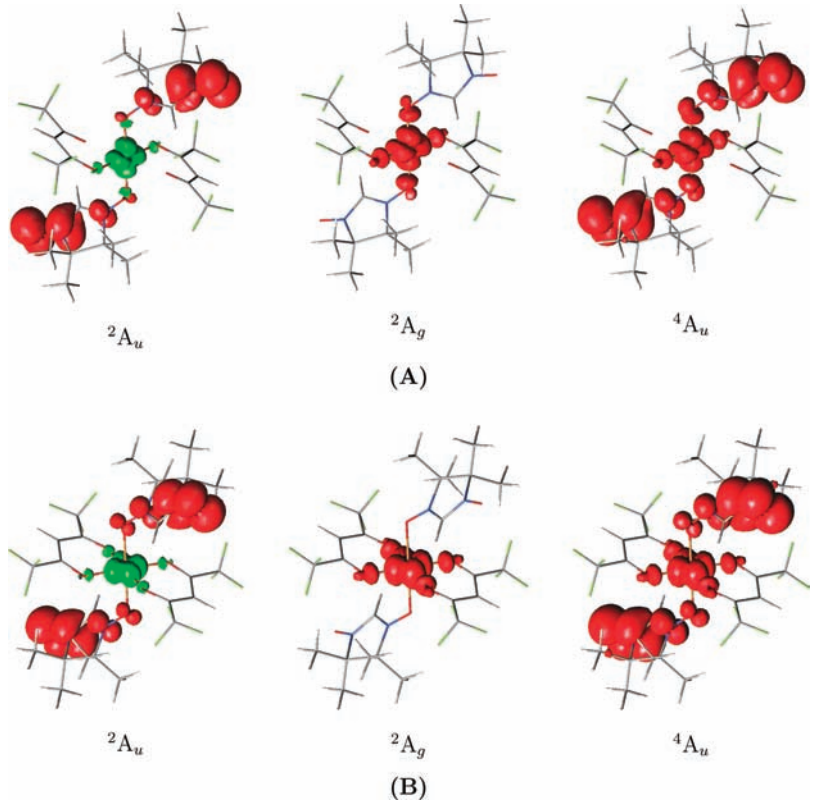

Figure 4. Spin density of the lowest ^2A_u, ^2A_g, ^4A_u states of model I: (A) low-*T* structure and (B) high-*T* structure.

TABLE 1: Relative Energies (cm^{-1}) and *g* Factors of the Lowest ^2A_g, ^2A_u, and ^4A_u States

	model I						model II		
	IPEA $\hat{H}^{(0)}$			original $\hat{H}^{(0)}$			original $\hat{H}^{(0)}$		
	^2A_u	^2A_g	^4A_u	^2A_u	^2A_g	^4A_u	^2A_u	^2A_g	^4A_u
				Low-*T* Structure					
CASSCF	0	150	213	0	150	213	0	129	184
CASPT2	0	215	759	0	753	912	0	672	827
			752			906			820
CASPT2+SOC	0	211	753	0	749	907	0	668	821
$g_{\|\|}$	1.841	2.501	2.185	1.852	2.475	2.174	1.836	2.522	2.191
	1.986	2.058	2.029	1.986	2.058	2.027	1.971	2.097	2.041
$g_\perp$	1.951	2.157	2.063	1.955	2.149	2.059	1.970	2.104	2.046
g_{av}	1.926	2.239	2.092	1.931	2.227	2.087	1.926	2.241	2.093
				High-*T* Structure					
CASSCF	12	4	0	12	4	0	8	3	0
CASPT2	117	0	368	0	386	341	0	314	268
			366			338			266
CASPT2+SOC	119	0	367	0	383	339	0	312	266
$g_{\|\|}$	1.818	2.551	2.201	1.829	2.533	2.193	1.848	2.473	2.170
	1.962	2.114	2.049	1.964	2.111	2.047	1.965	2.089	2.037
$g_\perp$	1.965	2.123	2.050	1.967	2.119	2.048	1.974	2.116	2.047
g_{av}	1.915	2.263	2.100	1.920	2.254	2.096	1.929	2.226	2.085

oxygen p_σ partners), while the electron spins in the π^* orbitals on both nitroxides are coupled into a singlet, thus giving zero spin density in this region of space.

Table 1 includes the calculated splitting of the three lowest states $^2A_{u,g}$, ^4A_u originating from the three-spin exchange coupling in each model. As one can see, the splittings are only slightly affected (at most a few cm^{-1}) by spin orbit coupling. For the low-*T* structures, these splittings may be confronted to the energy level scheme presented in refs 2–4 based on a spin Hamiltonian for the case $|J| \gg B$, $J < 0$ (*J* corresponding to the exchange interaction between copper and each nitroxide). According to this scheme, the $^4A_u - ^2A_g$ splitting should correspond to $-J$, whereas the splitting between both doublet states should be twice as large, $-2J$. Absolute values of *J* ranging from 100 cm^{-1} to more than 150 cm^{-1} are reported in ref 3 For $Cu(hfac)_2L^{Pr}$, a $|J|$ value of at least 125 cm^{-1} is reported ($T <$ 90 K).

Looking first at the CASSCF results in Table 1, we note that the calculated splittings at this level of theory quite closely obey the spin-Hamiltonian scheme. However, the predicted $|J|$ values are too small: 63−75 cm^{-1} for model I and 55−65 cm^{-1} for model II. With CASPT2, the calculated splittings are very

strongly dependent on the type of $\hat{H}^{(0)}$ employed. In particular, the relative position of the ^2A_g state with respect to the other two states seems to be most sensitive. With respect to the lowest ^2A_u state, ^2A_g is shifted upward by more than 500 cm^{-1} when replacing the (standard) IPEA $\hat{H}^{(0)}$ by the original $\hat{H}^{(0)}$ in model I. The total, $^4A_u-^2A_u$ splitting is less affected (150 cm^{-1}). From this splitting, a $|J|$ value of 252 cm^{-1} (IPEA $\hat{H}^{(0)}$) or 304 cm^{-1} (original $\hat{H}^{(0)}$) may be deduced for the low-T structure of model I. Even if the latter value is probably too large, the original $\hat{H}^{(0)}$ results are on the whole more reliable, in that they at least qualitatively correspond to the expected spin-Hamiltonian scheme. When going to model II, the splittings obtained with the latter $\hat{H}^{(0)}$ are slightly reduced, giving a J value of 276 cm^{-1}.

For the high-T structures, CASSCF gives a ^4A_u ground state, thus predicting ferromagnetic coupling between the three spins, with a J value of +4 cm^{-1} (model I). The coupling becomes antiferromagnetic at the CASPT2 level; however, also here the position of ^2A_g with respect to the other two states is crucially dependent upon the type of $\hat{H}^{(0)}$ used. With the IPEA $\hat{H}^{(0)}$, the ^2A_g state in fact becomes the ground state, while, similar to the low-T structure, replacing this $\hat{H}^{(0)}$ by the original leads to an upward shift of this state by around 500 cm^{-1}, now placing it even higher than the ^4A_u state. When going to model II, the magnetic coupling is again slightly reduced. However, it is clear that the CASPT2 splittings in Table 1 are considerably too high as compared to the J values estimated from experiment; e.g., a J value of only -10 cm^{-1} is estimated for $Cu(hfac)_2L^{Bu}$ in ref 5.

In summary, the results presented in Table 1 indicate that CASPT2 may be able to give a qualitative explanation, yet not a quantitative description of the magnetic coupling in the considered spin triads. Since the correct relative splittings are obtained at the CASSCF level, the origin of the failure is in the perturbational approach of dynamic correlation. As was already noted in ref 23, the (standard) IPEA zeroth-order Hamiltonian is found to perform worse in this respect than the original $\hat{H}^{(0)}$. An improved description may be expected from multireference configuration interaction (MRCI) calculations. In particular, difference dedicated CI,[29–31] designed to obtain accurate energy differences rather than total energies, has been shown to provide precise data for the Heisenberg splitting in magnetically coupled dimers involving transition metals.[23,32–34] On the other hand, the inherent multideterminantal character of the magnetic exchange coupling in the present and other trinuclear complexes[35] prevents DFT from providing an appropriate description of the ground-state doublet, although an estimate of J may be obtained from a broken symmetry approach.[6,35,36]

3.2. *g* Factors. Table 1 also includes the calculated g factors for the three lowest states in each structure, based on CASSCF/CASPT2 data with the two different $\hat{H}^{(0)}$ approaches. All g factors exhibit a tetragonal layout; i.e., there are two values that are similar (the equatorial $g_\perp$) and one value that differs significantly from the others (the axial $g_{||}$, with an axis coinciding with the y-axis for the low-T structures and with the z-axis for the high-T structures). This conforms with the approximate tetragonal symmetry of the copper(II) environment. We note that each state is characterized by its own typical values of the g factors, independent of the model and the molecular cluster structure (low-T or high-T). The g factors of the ^2A_g state resemble those of a typical copper(II) in a tetragonal environment ($g > 2$). This is not surprising, as this state corresponds to a situation where the nitroxide spins are coupled as a singlet (cf. the spin density plots in Figure 4). The g factors of the ^2A_u and ^4A_u states are quite different, i.e., much closer to g_e and respectively below and above the free electron g_e value.

The calculated g values conform with the experimental observations, although also in this case the agreement is only qualitative. Importantly, our calculations confirm the observed "$g < 2$ signals" for the low-T structure,[2,3] thus confirming that ^2A_u should indeed be the ground-state at low temperature. However, the calculated g values in Table 1 are significantly smaller than the g values deduced from experiment.[3] This is particularly the case for $g_{||}$, with calculated values of 1.836−1.851, while the experimental data are all larger than 1.90, ranging between 1.905 and 1.909. For $g_\perp$ the correspondence is better. Here, experimental values are ranging between 1.974 and 1.998, whereas the calculated values in Table 1 are smaller by 10−30 ppt. With increasing temperature, EPR spectra of $Cu(hfac)_2L^R$ compounds typically show a pronounced shift toward higher g factors, getting broadened at the same time. This is caused by redistribution of the spin state populations with increasing temperature. At low temperatures, with $kT \gg |J|$, only the lowest ^2A_u state is populated. However, with increasing temperature and a simultaneous decrease of the exchange coupling, all three states get comparable populations at $kT > |J|$, the fast spin exchange process then leading to an averaging effect and the appearance of a single line in the "center of mass" of the EPR spectrum, shifted toward higher g values as compared to the low temperature signal.[4] Precise experimental data for the g factors of ^2A_g, ^4A_u states are therefore not provided. For the ^2A_g state, we expect the calculated $g_\perp$ and $g_{||}$ in Table 1 to be too high by up to 30 and 200 ppt, respectively. In a previous study of the g factors of $[Cu(NH_3)_4]^{2+}$, $[CuCl_4]^{2-}$, and plastocyanin,[20] we have shown that, with the active space used in the present work, the ground-state wave function obtained from CASSCF gives a too ionic description of the Cu−ligand interactions, by providing the SOMO (i.e., for example orbital $101a_g$ in Figure 3) with too much Cu 3d and too little ligand σ character. This then gives rise to too large angular momentum (L) and spin−orbit (SO) matrix elements in the expressions of the **g** tensor, leading to an overestimation of Δg with respect to the free-electron value. An improved description of the g values may be obtained by making use of PMCAS (perturbation modified CAS) rather than CASSCF wave functions for the calculation of the L and SO matrix elements. The PMCAS wave functions should be obtained from a multistate CASPT2 treatment,[37] including besides the LF states also the charge-transfer state involving the transition of an electron from the bonding orbital into the SOMO. However, in the present case, extending the number of excited states in the CASSCF calculations with the CT excitation out of the equatorial Oσ orbitals proved to be unfeasible in practice, due to the presence of several lower-lying CT states involving excitations out of the NOπ orbitals into either Cu 3d or NOπ*.

On the whole, quite similar results are obtained for each state at the different models/structures and with both $\hat{H}^{(0)}$ approaches. That the calculated g factors are reasonably independent of $\hat{H}^{(0)}$ is due to the fact that these factors are not affected by the relative energy of the three lowest spin states. Rather, for each of these states, contributions to Δg almost exclusively come from excited states with the same spin/symmetry. This is strictly true for the ^4A_u state, the g factors of which are calculated by means of a sum-over-states approach built on second-order perturbation theory (L matrix elements between states of different spin or symmetry being zero). For the ^2A_g, ^2A_u states, g factors are obtained starting from wave functions already including SOC

(still mixing only states with the same symmetry); however, as the effect of SOC is very small, the same consideration still holds.

The calculated ligand field excitation energies (not including SOC) are presented in Table 2. As one can see, the relative energies (within each column) of the two model I structures are to some extent dependent on $\hat{H}^{(0)}$, the original $\hat{H}^{(0)}$ giving results that are higher by 200−1000 cm^{-1}. As the excitation energies appear in the denominator of the different terms in a sum-over-states approach, this gives g factors systematically somewhat closer to the free-electron values with $\hat{H}^{(0)}$. We further note that the main contribution to $\Delta g_{||}$ comes from the excitation of an electron within the equatorial plane (i.e., $d_{yz} \rightarrow d_{y^2-z^2}$ in the low-T, $d_{xy} \rightarrow d_{x^2-y^2}$ in the high-T structures), while the main contributors to $\Delta g_{\perp}$ are the excitations out of the d_{π} orbitals (d_{xy},$d_{xz} \rightarrow d_{y^2-z^2}$ in the low-T, d_{xz},$d_{yz} \rightarrow d_{x^2-y^2}$ in the high-T structures). When comparing the ligand field spectrum of models I and II in Table 2, the most important differences are found for the high-T structures, displaying a considerably stronger ligand field in model II than in model I. This should be traced back to structural differences, in particular to the equatorial $Cu-O_{hfac}$ bonds being shorter by about 0.03 Å in the high-T model II structure [average $R(Cu-O_{hfac}) = 1.985$ Å] as compared to model II [average $R(Cu-O_{hfac}) = 1.996$ Å], while the axial $Cu-O_L$ bond is longer by 0.127 Å. These differences give rise to a considerably larger Jahn−Teller splitting in model II: 10 600 cm^{-1}, as compared to 6600 cm^{-1} in model I. The other three states, contributing most to Δg, are also shifted to higher energies by around 1500 cm^{-1}, thus producing g factors that are significantly closer to g_e for model II than for model I. The most important shift is found for the $g_{||}$ value of the ^2A_g state, which is decreased from 2.533 to 2.473, bringing it closer to the value to be expected for a six-coordinated $Cu(II)O_6$ environment. On the other hand, for the low-T structures, the calculated g factors for model II are slightly worse, i.e., further from g_e than for model I. This can again be related to a weaker ligand field in model II, although the differences between the excitation energies in Table 2 are in this case less pronounced. The shift to a weaker ligand field again conforms with the structural differences between both models, which are also less pronounced for the low-T structures, with longer equatorial Cu−O bonds (by 0.015 Å on the average) and a shorter $Cu-O_{hfac}$ bond (by 0.026 Å) in model II.

Finally, we note that the present results correspond to what can be expected for an exchange-coupled linear spin triad nitroxide−copper(II)−nitroxide, starting from a spin-Hamiltonian model.[4] Within such model, effective **g** tensors for the three spin states can be found from the $\mathbf{g}^{Cu}$ and (assumed) isotropic $\mathbf{g}^{L}$ tensor of copper(II) and nitroxide respectively as

$$\mathbf{g}^{^2A_u} = \frac{4g^L\mathbf{1} - \mathbf{g}^{Cu}}{3}$$

$$\mathbf{g}^{^2A_g} = \mathbf{g}^{Cu}$$

$$\mathbf{g}^{^4A_u} = \frac{2g^L\mathbf{1} + \mathbf{g}^{Cu}}{3}$$

Using average values of the different g factors in Table 1, i.e., 2.24 for ^2A_g, 1.92 for ^2A_u, and 2.09 for ^4A_u, gives $g_{av}^{Cu} = 2.24$ and $g^L = 2.005$, the latter value being very close to g_e, as expected for nitroxides. It should be noted though that our calculations do not explicitly include the main contributions to the individual nitroxide Δg, since the appropriate NO orbitals are not included in the CASSCF active space.

3.3. Magnetic Moments. Plots of the effective magnetic moment as a function of the temperature for both models are presented in Figure 5A. For each model, two plots are presented, obtained by using the calculated relative energies (CASPT2+SOC in Table 1) for either the low-T structure (blue) or for the high-T structure (red). An experimental plot of the $\mu_{eff}(T)$ dependence of $Cu(hfac)_2L^{Pr}$ is presented in ref 3. In ref 5, the experimental $\mu_{eff}(T)$ plot of $Cu(hfac)_2L^{Bu}0.5C_8H_{18}$ is compared to a simulated plot, based on the experimental $g_{eff}(T)$ dependence and making use of the spin-Hamiltonian formalism for a linear spin triad.

Each individual state has a magnetic moment that is proportional to its g factor (g_{av}) and spin. The size of the magnetic moment can be estimated from the relation $\mu = g[S(S+1)]^{0.5}\beta$, giving 1.732 β for a doublet and 3.873 β for a quartet state (with $g = g_e$). When the g factor deviates from g_e, this is reflected in a smaller or larger magnetic moment for a particular spin.

At low temperatures, when the thermal energy is smaller than the exchange interaction, the magnetic moment is solely determined by the ^2A_u ground state. With a g_{av} factor of around 1.93, the magnetic moment should go to 1.67 β as the temperature goes toward zero, conforming with the plots in Figure 5A. As the temperature is increased, the ^2A_g state becomes populated, and the magnetic moment increases toward the square root of the mean of χT for both doublets, i.e. around 1.80 β. Since, for model I, the relative energy of the ^2A_g state

TABLE 2: Calculated Spin-Free Ligand Field Spectrum (cm^{-1})

	model I						model II		
	IPEA $\hat{H}^{(0)}$			original $\hat{H}^{(0)}$			original $\hat{H}^{(0)}$		
soo[a]	^2A_u	^2A_g	^4A_u	^2A_u	^2A_g	^4A_u	^2A_u	^2A_g	^4A_u
				Low-T Structure					
$d_{y^2-z^2}$	0	215	759	0	753	912	0	672	827
d_{x^2}	10 844	10 773	11 127	11 634	11 894	11 906	10 519	10 766	10 803
d_{yz}	11 056	10 942	11 296	11 890	12 134	12 149	11 222	11 389	11 396
d_{π}[b]	12 434	12 260	12 581	13 359	13 453	13 462	13 018	13 135	13 151
d_{π}[b]	13 393	13 230	13 566	14 357	14 432	14 463	13 495	13 616	13 642
				High-T Structure					
$d_{x^2-y^2}$	0	−117	250	0	386	341	0	314	268
d_{z^2}	5 957	6 096	6 602	6 614	6 953	7 090	10 599	10 850	10 932
d_{xy}	10 147	9 997	10 374	10 802	10 911	10 933	12 250	12 331	12 346
d_{π}[b]	10 631	10 504	10 887	11 284	11 431	11 455	12 772	12 857	12 867
d_{π}[b]	10 926	10 772	11 144	11 606	11 705	11 724	13 125	13 192	13 200

[a] Character of the Cu 3d contribution in the singly occupied orbital. [b] Mixture of d_{xy}, d_{xz} in the low-T structures and of d_{xz}, d_{yz} in the high-T structures.

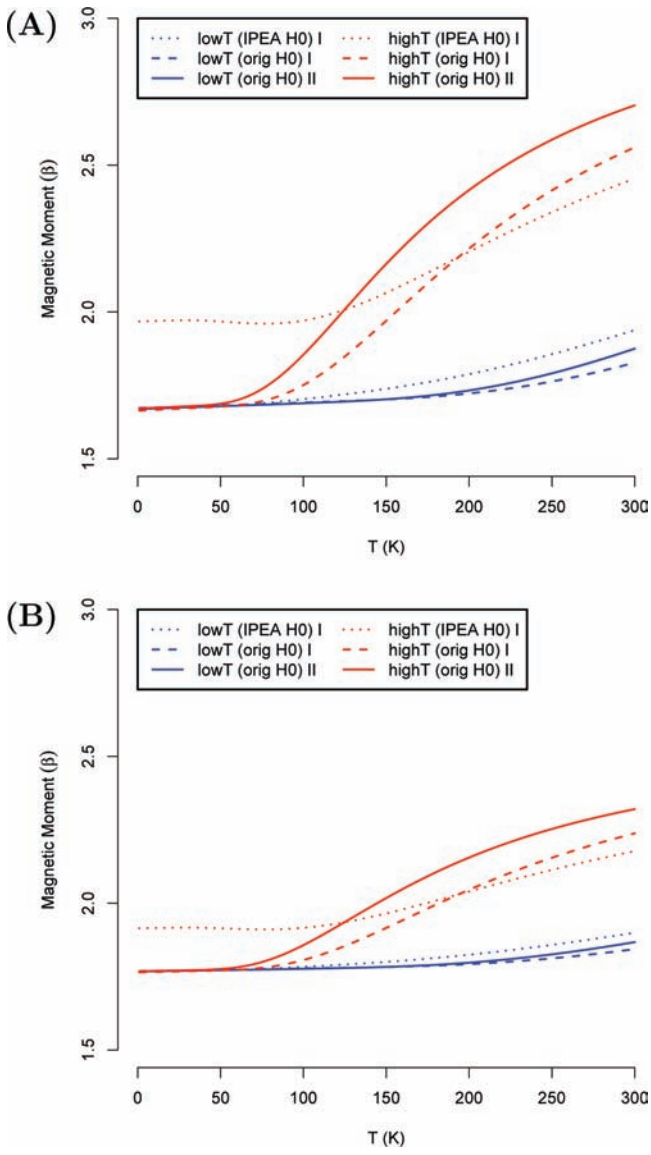

Figure 5. Temperature dependence $\mu_{eff}(T)$ of the magnetic moment of the spin triad, based on the calculated splittings between the SO states obtained for the low-T (blue) and high-T structures (red). (A) only the CuO_6 units. (B) Accounting for the presence of one-spin CuO_4N_6 units in the $Cu(hfac)_2L^{Pr}$ crystals.

is much higher with the original $\hat{H}^{(0)}$ (749 cm^{-1}) than with the IPEA $\hat{H}^{(0)}$ (211 cm^{-1}) (see Table 1), a steeper increase of the μ_{eff} curve is predicted with the latter approach. For model II, a slightly smaller exchange interaction is predicted than for model I (both with the original $\hat{H}^{(0)}$). As such, the corresponding $\mu_{eff}(T)$ (blue) curve in Figure 5A is slightly steeper. Our calculations do not predict a significant role for the ^4A_u state in the low-T region, as its energy is too high (752−907 cm^{-1}) to give this state a significant population.

In the high-temperature limit, with all three SO states becoming equally populated, the magnetic moment should level off to the square root of the mean of χT for the three states, i.e. 2.76 β. As the (red) plots indicate, this value is in fact not reached below 300 K. The largest values of μ_{eff} are calculated for model II, conforming with the fact that the exchange coupling for the high-T structure of this model is significantly weaker than for model I. For the latter model, slightly larger μ_{eff} are obtained with the original than with the IPEA $\hat{H}^{(0)}$. This should be traced back to the fact that the ^4A_u state is predicted at slighly lower energies, thus giving a more important contribution.

The plots provided in Figure 5A obviously can only provide a (qualitative) explanation for the relative values of the observed magnetic moments of $Cu(hfac)_2L^{Pr}$ in a limited temperature region around either 115 or 293 K, i.e., the temperatures at which the X-ray structures were obtained, based on which the model II low-T and high-T structures were constructed. In the intermediate region, X-ray data reveal the occurrence of a gradually increasing $Cu-O_L$ distance with temperature[3] (with a structural phase transition occurring at $T = 226$ K), with a concomitant decrease of the exchange interaction J. This gives rise to a (more or less, depending on the character of R) an abrupt change in the magnetic moment in the intermediate region, crossing from the blue to the red curve in Figure 5A.

Before comparing the calculated results to the experimental $\mu_{eff}(T)$ plot of $Cu(hfac)_2L^{Pr}$, given in ref 3, we have to account for the occurrence of a second type of copper center in the crystals, i.e., a one-spin CuO_4N_2 unit with $g_{av} = 2.148$ (taken from the experimental EPR spectrum at 260 K),[2] thus giving a constant magnetic moment of 1.86 β. The resulting plot is shown in Figure 5B. At low temperatures (<70 K), the experminental plot indicates a value of $\mu_{eff} = 1.82$ β. The calculated magnetic moments for the low-T structures in this temperature range are too small, conforming with the fact that the g factors of the ^2A_u state are underestimated by the calculations. At high temperatures (>260 K), the experimental magnetic moment reaches a constant value near 2.6 β, much higher than the calculated magnetic moment. This is again to be expected, since the splittings between the three lowest SO states obtained from CASPT2 are too large with respect to the experimentally derived values of J, leading to an underestimation of the contribution of the excited doublet and (especially) quartet to the magnetic moment.

Conclusion

In this work we have reported the results of a multiconfigurational ab initio study of electron spin exchange interactions in nitroxide−Cu(II)−nitroxide three-spin systems occurring in $Cu(hfac)_2L^{Pr}$ crystals. The experimentally observed thermally induced structural changes of the CuO_6 units in these crystals were related to the occurrence of two distinct electronic structures at either a short or longer $Cu-O_L$ distance, giving rise to two close-lying minima in the electronic energy profile along the $Cu-O_L$ axis (Figure 2). The difference in electronic structure is due to the different character of the Cu 3d SOMO at the two minima: $d_{x^2-y^2}$ at long $R(Cu-O_L)$ (high-T) structure, $d_{y^2-z^2}$ at short $R(Cu-O_L)$ (low-T structure). The latter orbital is involved in a (weak) covalent interaction with the a_g NOπ^* combination, thus explaining the stronger exchange coupling in the low-T structure.

The strengths and weaknesses of the CASPT2 method in calculating the magnetic properties associated with the two different electronic structures were critically examined. An important problem with the method is its inability to reproduce the expected splitting pattern between the three spin states ^2A_u, ^2A_g, and ^4A_u associated with the ground-state configuration of the considered symmetric spin-triad. As already concluded previously,[23] the original zeroth-order Hamiltonian is found to perform better in this respect than the IPEA-modified $\hat{H}^{(0)}$. An estimate of the coupling parameter J may be obtained from the $^4A_u-^2A_u$ splitting, but it is clearly overestimated. This is opposed to the CASSCF results, showing the correct splitting pattern but underestimating the size of the exchange coupling. The

problem with CASPT2 in describing magnetic couplings is also reflected in its inability to correctly reproduce the experimentally observed $\mu_{eff}(T)$ dependence, in particular in the high-T region.

Our calculations undisputably point to a ^2A_u ground-state at low temperatures, giving rise to the "unusual" $g < 2$ signals in the low-T Cu(hfac)$_2$L^{Pr} EPR spectrum. The calculated Δg values for all three states were found to be qualitatively correct but are in general slightly too large. As discussed in detail previously,[20,38] this is caused by a too ionic description of the Cu−O bonds at the CASSCF level. However, we would like to stress that the results presented in this work are on the edge of what can be achieved in this field with today's ab initio quantum chemical methods. The present CASSCF/CASPT2 methodology opens up a wide range of applications in the study of the electronic structure and g factors of inorganic and bioinorganic three-spin systems, such as, for example, tris-hydroxy-bridged Cu(II) centers and the intermediates in the catalytic cycle of multicopper oxidases,[39,40] which are the subject of a forthcoming publication.[41]

Acknowledgment. This investigation has been supported by grants from the Flemish Science Foundation (FWO), from the Concerted Research Action of the Flemish Government (GOA), and from MSMT CR (LC512).

References and Notes

(1) Ovcharenko, V. I.; Fokin, S. V.; Romanenko, G. V.; Shvedenkov, Y. G.; Ikorskii, V. N.; Tretuakov, E. V.; Vasilevskii, S. F. *J. Struct. Chem.* **2002**, *43*, 153–167.

(2) Fedin, M. V.; Veber, S. L.; Gromov, I. A.; Ovcharenko, V. I.; Sagdeev, R. Z.; Schweiger, A.; Bagryanskaya, E. G. *J. Phys. Chem. A* **2006**, *110*, 2315–2317.

(3) Fedin, M.; Veber, S.; Gromov, I.; Maryunina, K.; Fokin, S.; Romanenko, G.; Sagdeev, R.; Ovcharenko, V.; Bagryanskaya, E. *Inorg. Chem.* **2007**, *46*, 11405–11415.

(4) Fedin, M. V.; Veber, S. L.; Gromov, I. A.; Ovcharenko, V. I.; Sagdeev, R. Z.; Bagryanskaya, E. G. *J. Phys. Chem. A* **2007**, *111*, 4449–4455.

(5) Veber, S. L.; Fedin, M. V.; Potapov, A. I.; Maryunina, K. Y.; Romanenko, G. V.; Sagdeev, R. Z.; Ovcharenko, V. I.; Goldfarb, D.; Bagryanskaya, E. G. *J. Am. Chem. Soc.* **2008**, *130*, 2444–2445.

(6) Ovcharenko, V. I.; Romanenko, G. V.; Maryunina, K. Y.; Bogomyakov, A. S.; Gorelik, E. V. *Inorg. Chem.* **2008**, *47*, 9537–9552.

(7) Fedin, M.; Ovcharenko, V.; Sagdeev, R.; Reijerse, E.; Lubitz, W.; Bagryanskaya, E. *Angew. Chem., Int. Ed.* **2008**, *47*, 6897–6899.

(8) Andersson, K.; Malmqvist, P.-Å.; Roos, B. O. *J. Chem. Phys.* **1992**, *96*, 1218.

(9) Malmqvist, P. Å.; Roos, B. O.; Schimmelpfennig, B. *Chem. Phys. Lett.* **2002**, *357*, 230–240.

(10) Ahlrichs, R.; Bär, M.; Häser, M.; Kölmel, C. *Chem. Phys. Lett.* **1989**, *162*, 165.

(11) Perdew, J. P.; Burke, K.; Ernzerhof, M. *Phys. Rev. Lett.* **1996**, *77*, 3865.

(12) Perdew, J. P.; Ernzerhof, M.; Burke, K. *J. Chem. Phys.* **1996**, *105*, 9982.

(13) Weigend, F.; Ahlrichs, R. *Phys. Chem. Chem. Phys.* **2005**, *7*, 3297–3305.

(14) Pierloot, K.; Dumez, B.; Widmark, P.-O.; Roos, B. O. *Theor. Chim. Acta* **1995**, *90*, 87–114.

(15) Forsberg, N.; Malmqvist, P.-Å. *Chem. Phys. Lett.* **1997**, *274*, 196.

(16) Karlström, G.; Lindh, R.; Malmqvist, P.-Å.; Roos, B. O.; Ryde, U.; Veryazov, V.; Widmark, P.-O.; Cossi, M.; Schimmelpfennig, B.; Neogrady, P.; Seijo, L. *Comput. Mater. Sci.* **2003**, *28*, 222.

(17) Pierloot, K. In *Computational Organometallic Chemistry*; Cundari, T. R. Ed.; Marcel Dekker, Inc.: New York, 2001; pp 123−158.

(18) Pierloot, K. *Mol. Phys.* **2003**, *101*, 2083–2094.

(19) Pierloot, K. In *Computational Photochemistry, 16*; Olivucci, M. Ed.; Elsevier: New York, 2005; pp 279−315.

(20) Vancoillie, S.; Pierloot, K. *J. Phys. Chem. A* **2008**, *112*, 4011–4019.

(21) Andersson, K.; Malmqvist, P.-Å.; Roos, B. O.; Sadlej, A. J.; Wolinski, K. *J. Chem. Phys.* **1990**, *94*, 5483.

(22) Ghigo, G.; Roos, B. O.; Malmqvist, P.-Å. *Chem. Phys. Lett.* **2004**, *396*, 142–149.

(23) Queralt, N.; Taratiel, D.; de Graaf, C.; Caballol, R.; Cimiraglia, R.; Angeli, C. *J. Comput. Chem.* **2008**, *29*, 884–1003.

(24) Malmqvist, P. Å.; Roos, B. O. *Chem. Phys. Lett.* **1989**, *155*, 189–194.

(25) Hess, B. A.; Marian, C. M.; Wahlgren, U.; Gropen, O. *Chem. Phys. Lett.* **1996**, *251*, 365–371.

(26) Christiansen, O.; Gauss, J.; Schimmelpfennig, B. *Phys. Chem. Chem. Phys.* **2000**, *2*, 965–971.

(27) Vahtras, O.; Engström, M.; Schimmelpfennig, B. *Chem. Phys. Lett.* **2002**, *351*, 424–430.

(28) Vancoillie, S.; Malmqvist, P.-Å.; Pierloot, K. *ChemPhysChem* **2007**, *8*, 1803–1815.

(29) Miralles, J.; Daudey, J.-P.; Caballol, R. *Chem. Phys. Lett.* **1992**, *198*, 555.

(30) Miralles, J.; Castell, O.; Caballol, R.; Malrieu, J.-P. *Chem. Phys.* **1993**, *172*, 33–43.

(31) Neese, F. *J. Chem. Phys.* **2003**, *119*, 9428–9443.

(32) Herebian, D.; Wieghardt, K. E.; Neese, F. *J. Am. Chem. Soc.* **2003**, *125*, 10997–11005.

(33) Bordas, E.; Caballol, R.; de Graaf, C. *J. Mol. Struct. (Theochem)* **2005**, *727*, 173–179.

(34) Negodaev, I.; de Graaf, C.; Caballol, R. *Chem. Phys. Lett.* **2008**, *458*, 290–294.

(35) Noh, E. A. A.; Zhang, *J. Chem. Phys.* **2006**, *330*, 82–89.

(36) Ruiz, E.; Rodríguez-Fortea, A.; Cano, J.; Alvarez, S.; Alemany, P. *J. Comput. Chem.* **2003**, *24*, 982–989.

(37) Finley, J.; Malmqvist, P.-Å.; Roos, B. O.; Serrano-Andrés, L. *Chem. Phys. Lett.* **1998**, *288*, 299–306.

(38) Solomon, E. I.; Szilagyi, R. K.; DeBeer George, S.; Basumallick, L. *Chem. Rev.* **2004**, *104*, 419–458.

(39) Yoon, J.; Mirica, L. M.; Stack, T. D. P.; Solomon, E. I. *J. Am. Chem. Soc.* **2005**, *127*, 13680–13693.

(40) Chalupský, J.; Neese, F.; Solomon, E. I.; Ryde, U.; Rulíšek, L. *Inorg. Chem.* **2006**, *45*, 11051–11059.

(41) Vancoillie, S.; Chalupský, J.; Ryde, U.; Solomon, E. I.; Neese, F.; Pierloot, K.; Rulíšek, L. Manuscript in preparation.

JP900822V